AGU PUBLICATIONS

Geophysical Research Letters

RESEARCH LETTER
10.1002/2016GL069909

Key Points:
- A new metric, contribution-weighted rain rate, is proposed to characterize the climatology of tropical rain
- At 0.25° × 0.25° resolution, and 3-hourly temporal resolution, half the rain falls in 1% of the area of the tropics
- The spectrum of contribution-weighted rain rate is nearly lognormal

Supporting Information:
- Supporting Information S1

Correspondence to:
V. Venugopal,
venu.vuruputur@gmail.com

Citation:
Venugopal, V., and J. M. Wallace (2016), Climatology of contribution-weighted tropical rain rates based on TRMM 3B42, *Geophys. Res. Lett.*, *43*, 10,439–10,447, doi:10.1002/2016GL069909.

Received 6 JUN 2016
Accepted 7 SEP 2016
Accepted article online 12 SEP 2016
Published online 6 OCT 2016

Climatology of contribution-weighted tropical rain rates based on TRMM 3B42

V. Venugopal[1] and J. M. Wallace[2]

[1]Centre for Atmospheric and Oceanic Sciences, & Divecha Centre for Climate Change, Indian Institute of Science, Bengaluru, India, [2]Department of Atmospheric Sciences, University of Washington, Seattle, Washington, USA

Abstract The climatology of annual mean tropical rain rate is investigated based on merged Tropical Rainfall Measuring Mission (TRMM) 3B42 data. At 0.25° × 0.25° spatial resolution, and 3-hourly temporal resolution, half the rain is concentrated within only ~1% of the area of the tropics at any given instant. When plotted as a function of logarithm of rain rate, the cumulative contribution of rate-ranked rain occurrences to the annual mean rainfall in each grid box is S shaped and its derivative, the contribution-weighted rain rate spectrum, is Gaussian shaped. The 50% intercept of the cumulative contribution R_{50} is almost equivalent to the contribution-weighted mean logarithmic rain rate $\overline{R_L}$ based on all significant rain occurrences. The spatial patterns of R_{50} and $\overline{R_L}$ are similar to those obtained by mapping the fraction of the annual accumulation explained by rain occurrences with rates above various specified thresholds. The geographical distribution of R_{50} confirms the existence of patterns noted in prior analyses based on TRMM precipitation radar data and reveals several previously unnoticed features.

1. Introduction

At any given time, it is raining over a small fraction of the tropics, and at any given place, it may rain only a small fraction of the time. Furthermore, rain rate, conditional upon the occurrence of rain, is positively skewed, with light rain much more common than downpours. It follows that most tropical rainfall is concentrated within a very small segment of the space-time domain: just how concentrated remains uncertain.

Dai [2001] analyzed global ground-based surface observations of the occurrence of continuous rain or snow, showers, and drizzle. On the basis of his results, *Trenberth et al.* [2003] estimated that at any given time, it is raining (not including drizzle) over ~6% of the area of the tropics. Hence, the rainfall rate (or intensity), conditional upon when it is raining, is more than an order of magnitude higher than the (unconditional) tropically averaged rain rate. A limitation of studies based on surface observations is the lack of quantitative data on rain rate. Moreover, the patterns of spatial variability of rainfall cannot be accurately captured by in situ observations. Hourly surface observations (e.g., from airports) contain quantitative information and hence could be a valuable resource for studies of rainfall characteristics [e.g., see *Higgins et al.*, 1996]; however, such data are not widely available in the tropics.

Satellite-based rainfall estimates are well suited for documenting rain rates because they are quantitative as well as spatially comprehensive. Since its inception in January 1998, NASA's Tropical Rainfall Measurement Mission (TRMM) [*Simpson et al.*, 1996; *Adler et al.*, 2000] has provided an unprecedented view of the space-time distribution of tropical rain. To date, most TRMM-based documentations of rain rate and rain frequency have been based on its precipitation radar (PR) data, which have a nominal resolution of ~5 km, with a sampling interval of ~3 days. The TRMM record is about 16 years long, yielding ~2000 PR samples at each location. Because the radar data are restricted to 215 km wide swaths, the analysis of these data is rather involved. For a comprehensive review of the findings based on the analysis of TRMM PR data, the reader is referred to *Houze et al.* [2015].

Biasutti et al. [2012] and *Biasutti and Yuter* [2013] documented the geographical distribution of tropical rain frequency and rain rate based on TRMM PR retrievals. They found that conditional rain rate (the rain rate when it is raining) is highly correlated with mean daily rainfall, while rain frequency (the fraction of TRMM PR overpasses with rain, irrespective of rain rate) is more highly correlated with climatological mean rainfall. They noted that rain frequency exhibits sharper spatial gradients than conditional rain rate and that some semiarid regions with infrequent occurrences of rain exhibit high conditional rain rates. *Yang and Nesbitt* [2014]

reported that ~3% of the TRMM data are raining pixels, about half as many as reported by *Trenberth et al.* [2003] on the basis of surface synoptic reports. That the rain is more concentrated in the PR data presumably reflects the fact that the observations are virtually instantaneous.

To overcome the limited spatial sampling of the TRMM PR data and to extend the range of applications of the TRMM products, algorithms have been developed that merge the PR data with data from infrared and microwave sensors carried aboard an array of polar orbiting and geostationary satellites, calibrated continuously in real time using rain gauge data. The most widely used of these data sets are the TRMM Multisatellite Precipitation Analysis (TMPA) products developed by the staff of the Mesoscale Atmospheric Processes Laboratory at NASA Goddard Space Flight Center [*Huffman et al.*, 2007; *Huffman and Bolvin*, 2013]. The research quality data set, labeled 3B42, provides precipitation estimates at 3-hourly resolution on a 0.25°×0.25° grid, yielding ~40,000 time samples (over the 15 year record) at each grid point, about 20 times as many as TRMM PR. An additional advantage of the merged data set is that being a simple space/time array, it is more straightforward to process and hence more accessible. The disadvantage of 3B42, in addition to its much coarser spatial resolution, is that it is a blended product whose error characteristics are difficult to quantify and have changed with time with the increasing availability of microwave observations. TRMM has recently been succeeded by the Global Precipitation Measurement Mission (GPM) for which there exists a blended product (Integrated MultisatellitE Retrievals for GPM) [*Huffman et al.*, 2015] analogous to 3B42 but available on a 0.1° × 0.1° grid with half hourly time resolution.

In this study we will make use of both TRMM and GPM merged data to determine the extent of the skewness of the frequency distribution of tropical rainfall in space and in time and to document the geographical distribution of conditional rain rate in greater detail than is possible using the PR data alone. The merged data sets are superior in this regard by virtue of their much more extensive coverage in space and time.

Rather than analyzing the frequency of rain occurrences with rates in various ranges, we consider the contribution of rain occurrences with rates in various ranges of rain rate to the climatological-mean annual accumulation. *Liu* [2011] employed a similar approach in his study of precipitation features revealed by TRMM Microwave Imager (TMI) and PR data sets. To emphasize this distinction, we will use the qualifier *contribution weighted* in referring to cumulative distributions or spectra based on contributions to annual accumulation rather than fraction of rain occurrences.

To avoid ambiguity in distinguishing between raining and non-raining pixels, we employ a "top down" approach, considering only the heavier rain events. As in *Liu* [2011], we make extensive use of what we will refer to as the 50% *intercept*. Rain events with rates higher than this value account for 50% of the annual contribution. As in *Watterson and Dix* [2003] and *Pendergrass and Hartmann* [2014], we plot the rain rate spectrum on a logarithmic scale in order to achieve a more uniform sampling.

We will discuss the data sets in the next section. Methodology and results are presented in sections 3 and 4 and sensitivity issues are addressed in section 5. Results are summarized and discussed in section 6, and we offer a few concluding remarks in section 7.

2. Data

Most of the analysis in this study is based on version 7 of the TRMM 3B42 merged product at 0.25° × 0.25° spatial resolution, 8 times daily, 50°N–50°S, for the 15 year record 1998–2012. For further documentation see http://trmm.gsfc.nasa.gov/3b42.html. Several validation studies of the TRMM 3B42 (v6 and v7) rainfall data have been performed using ground-based observations, and the rainfall estimates are generally considered to be reliable [e.g., *Dinku et al.*, 2007; *Chokngamwong and Chiu*, 2008; *Rahman et al.*, 2009; *Sapiano and Arkin*, 2009; *Roca et al.*, 2011], especially at the larger space scales and longer time scales [e.g., see *Huffman et al.*, 2007].

For the past 2 years NASA and JAXA's Global Precipitation Mission (GPM) *Hou et al.*, 2014] has been providing rainfall estimates on a 0.1° × 0.1° grid at 30 min intervals [*Huffman et al.*, 2015], resolving localized patches of heavy rainfall within mesoscale convective systems [e.g., *Liu and Zipser*, 2015] in greater detail than is afforded by TRMM retrievals. Because the GPM climatology extends only over 1 year, it is considered preliminary at this point. Both the TRMM and GPM data sets are available from NASAs Precipitation Measurement Missions web site at http://pmm.nasa.gov/data-access/downloads/{trmm,gpm}.

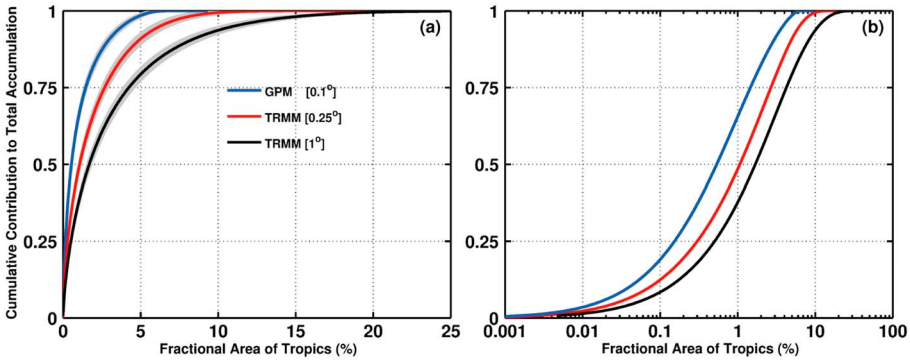

Figure 1. Cumulative contribution of grid boxes with the highest to lowest rain rates, to the instantaneous total tropical rainfall accumulation as a function of the fractional area of the tropics (30°S–30°N). The shaded regions around each curve in Figure 1a indicate their respective "snapshot-to snap-shot" 1 standard deviations. The estimates are based on TRMM 3B42V7 (1998–2012; 0.25° × 0.25°, 3-hourly; red solid curve), and GPM (April 2014 - March 2015, 0.1° × 0.1°, half-hourly; blue solid curve) retrieved rainfall. The 1°×1° TRMM data, for which the cumulative contribution is indicated by the black solid curve, was generated by smoothing the 0.25° × 0.25° data. In Figure 1a, the fractional area is plotted on a linear scale; in Figure 1b, it is plotted on a log scale to show more clearly the contribution of the heaviest rain rates.

In the TRMM 3B42 data, rain rates are expressed in millimeters per 3 h (i.e., the interval between successive maps) so that when the rain rates are summed in time, they yield the accumulated rainfall. However, in reality, the satellite observations from which the merged data are constructed are virtually instantaneous (albeit not simultaneous). Hence, we interpret and refer to the successive 3-hourly maps as "snapshots" and express the rain rates in units of mm h^{-1}.

We will define the tropics as 30°N–30°S, and in addressing the questions posed above, we do not stratify the data regionally, or by season, or by time of day. Thus, the number of samples available for our analysis, for TRMM 0.25° × 0.25°, 3-hourly observations are ~40,000 in time (15 years × 365 days × 8 snapshots/day) and ~300,000 in space (240 (30°S–30°N) × 1440 (0°–360°) grid boxes).

3. Spatial Distributions

In this section we estimate the fractional area of the tropics (30°S–30°N) that contributes to a specified percentage of total (spatially integrated) accumulation per snapshot. To estimate this fraction, for each snapshot rain rates in space are sorted from highest to lowest in magnitude. Let N represent the total number of grid boxes in the tropics for each snapshot (~300,000 at 0.25° × 0.25° resolution for TRMM), p be a specified percentage of the total tropical rainfall, and $n(p)$ be the number of grid boxes in the ranking (starting from the heaviest rain occurrence) required to account for p percent of the rainfall in that particular snapshot. If we ignore the weak latitudinal dependence of the areas of the grid boxes, the ratio $\frac{n(p)}{N}$ is equivalent to the areal fraction of the tropics that accounts for p percent of the accumulation in that particular snapshot; the curve of $\frac{n(p)}{N}$ plotted as a function of p is thus the (top-down) cumulative distribution of the fractional contribution to tropical rainfall. Repeating this procedure for all available snapshots (15 years of 3-hourly snapshots for TRMM; 1 year of 30 min snapshots for GPM), we obtain the climatological composite curves shown in Figure 1. The results shown in Figure 1 are for three different spatial resolutions, as indicated, and the shaded band centered on each curve (in Figure 1a) shows the corresponding (snapshot-to-snapshot) standard deviation. In the 0.25°×0.25° TRMM data, the fractional area of the tropics required to account for 50% of the total tropical rainfall is ~1%; for the degraded 1°×1° resolution TRMM data it is ~1.5%, and for the 0.1°×0.1° GPM data it is ~0.5%. (Figure 1b shows these cumulative curves as a function of log (fractional area) to highlight the contribution of the heaviest rain rates, i.e., the lower left end.) Hence, increasing the spatial resolution sharpens the frequency distribution but not dramatically. That the standard deviations are small suggests that these estimates are very tightly bound and validates our approach of considering all snapshots as nearly equivalent realizations or samples from a "universal" probability distribution of tropical rain rate.

4. Temporal Distributions

In this section, we proceed in the same manner as in the previous one, but in the time domain. We begin by calculating the fraction of the 365 days × 8/day = 2920) "snapshots" at 3-hourly intervals in the TRMM data

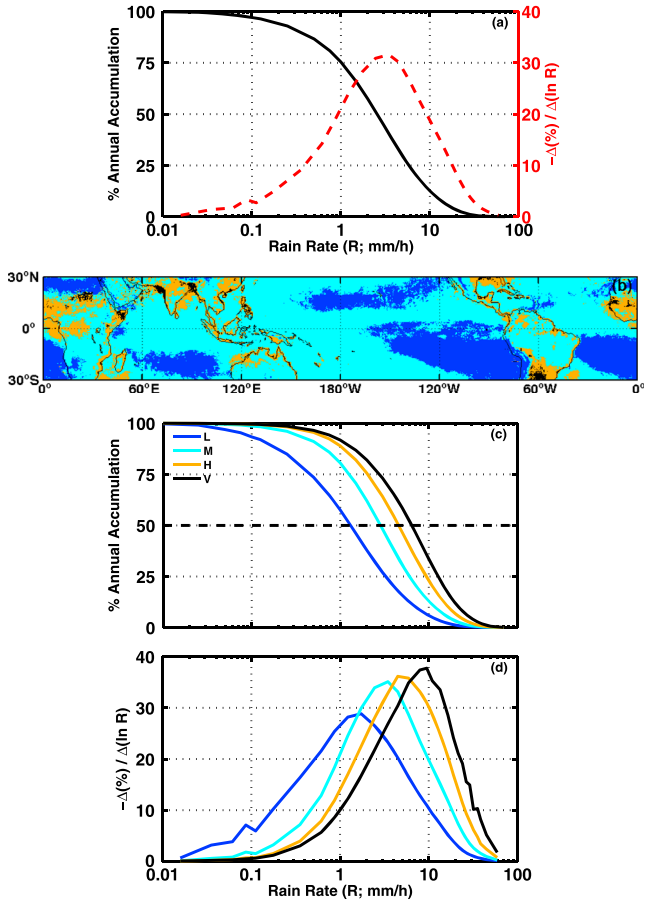

Figure 2. (a) Composite of the fractional contribution of rain rates higher than specified thresholds to the total annual accumulation at each grid in the tropics (30°S–30°N; solid black curve; ordinate on the left), and its (sign-reversed) derivative with respect to ln(rain rate) (dashed red curve; ordinate on the right). (b) Map of four regimes with the following rain rate partitioning: Low (<2 mm h^{-1}, L, blue); moderate (2–4 mm h^{-1}, M, cyan); heavy (4–6 mm h^{-1}, H, orange); and very heavy (>6 mm h^{-1}, V, black). (c and d) Same as the solid and dashed curves in Figure 2a, respectively, but estimated for the four regimes shown in Figure 2b. Based on 15 years (1998–2012) of TRMM 3B42V7 (0.25° × 0.25°, 3-hourly) rainfall data.

that contributes to a specified percentage of total annual accumulation in each grid box. For each grid box we (i) rank the 2920 rain rates, (ii) determine the numbers of snapshots required to account for specified fractions of the total annual accumulation in that grid box to create a "top down" cumulative contribution curve, and (iii) average these curves over all tropical grid boxes to obtain a single composite curve. When this composite curve is plotted as a function of rain rate on a logarithmic scale, as shown in Figure 2a, it is S shaped and nearly symmetric with respect to the 50% intercept, which corresponds to a rain rate of ~3 mm h^{-1}: rain events with rates heavier than this value account for half the annual accumulation. The cumulative contribution curves for individual grid boxes are also S shaped; however, they exhibit a range of 50% intercepts, as illustrated by the curves shown in Figure 2c, which are composites for grid boxes grouped according to the following four ranges of R_{50} (shown as a four-color map in Figure 2b): (i) *very heavy* V>6 mm h^{-1} (black in Figure 2b), (ii) *heavy* H 4–6 mm h^{-1} (orange), (iii) *moderate* M 2–4 mmh^{-1} (cyan), and (iv) *light* L<2 mm h^{-1} (blue).

The derivative of the cumulative contribution curves (with sign reversed) with respect to the natural log of rain rate corresponds to the *rain rate spectrum* (the dashed curve in Figure 2a): the fractional contribution to the annual mean rainfall from events with rates that fall within any specified range of rain rates is proportional to the area under this curve. It exhibits a Gaussian shape with a mode around 3 mm h^{-1}, which is approximately the same value as the 50% intercept R_{50}. In a similar manner, each of the four S shaped curves in Figure 2c can be differentiated to obtain the corresponding rain rate spectra shown in Figure 2d, whose modes closely match the corresponding 50% intercepts in Figure 2c.

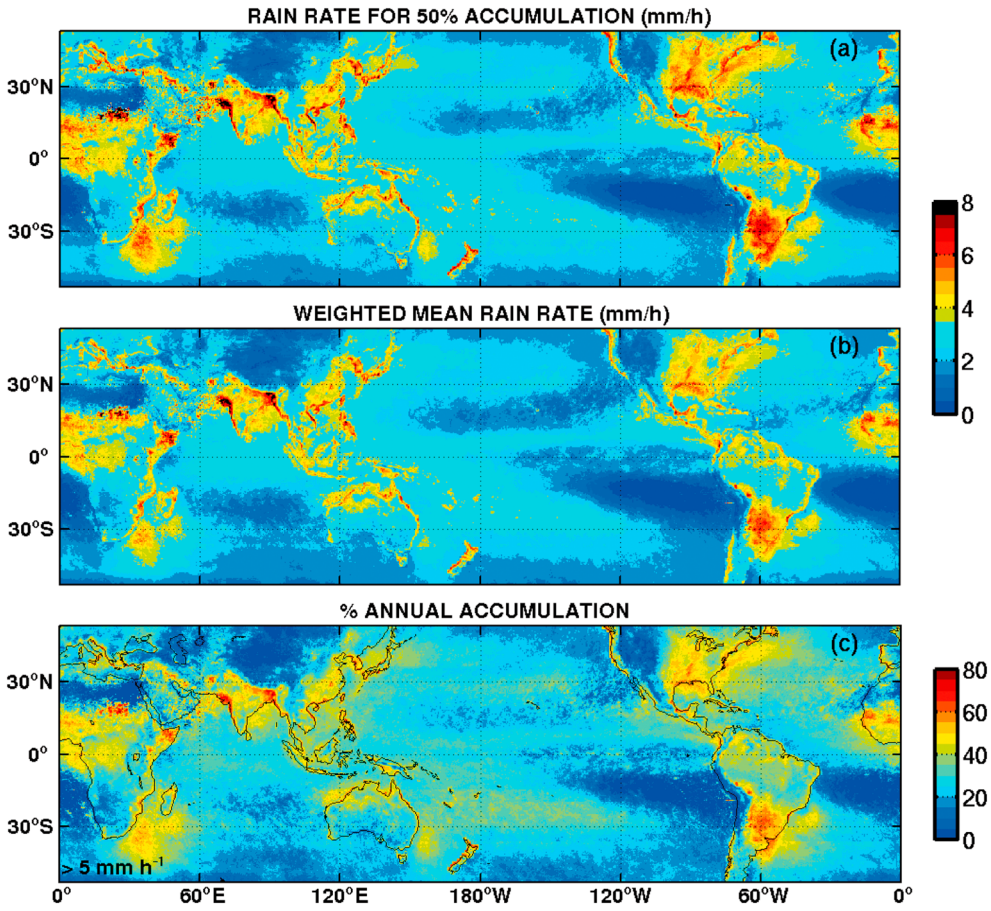

Figure 3. Spatial distribution of (a) the 50% intercept rain rate R_{50} (mm h^{-1}). Rain events with rates above this value account for half the annual accumulation; (b) weighted logarithmic mean rain rate ($\overline{R_L}$; see text for further details); and (c) the fraction (in %) of the annual accumulation explained by rain rates higher than 5 mm h^{-1}. Based on 15 years (1998–2012) of TRMM 3B42V7 (0.25° × 0.25°, 3-hourly) rainfall data.

As stated earlier, the geographical distribution of the grid boxes used in generating the four composite cumulative contribution curves in Figure 2c is shown in Figure 2b. The categories, based on rain rate at the 50% intercept R_{50}, expressed in mm h^{-1} correspond to (i) V: localized "hot spots," mostly over land, that include regions of orographically enhanced rainfall and regions subject to intense convective storms; (ii) H: most tropical land and some adjacent ocean areas, (iii) M: the oceanic convergence zones and tropical rainforests, and (iv) L : the equatorial dry zones and the core areas of the deserts.

A map of R_{50} for each grid box, shown in Figure 3a, provides a more detailed view of the geographical distribution of rain rate. *Liu* [2011] used analogous plots based on 50% contributions to the annual accumulation to document the geographical distributions of sizes, echo tops, and other properties of precipitation features in the TRMM PR and microwave data.

Figure 3b shows the geographical distribution of the logarithmic-mean rain rate, $\overline{R_L}$, i.e., the antilog of R-weighted log R, averaged over nearly all rain occurrences; to avoid ambiguity, the summation in the calculation of the weighted mean is truncated at 99% of the annual accumulation so that the lightest rain rates are not considered. That the geographical distribution and numerical values of logarithmic-mean rain rate are very similar to those of R_{50} shown in Figure 3a confirms that the distribution of rain rate is nearly lognormal. Similar patterns can be obtained by plotting the fractions of the annual accumulation attributable to rain occurrences with rates in excess of specified thresholds. Figure 3c shows such an exceedance map for 5 mm h^{-1} and the corresponding maps for 10, 20, and 30 mm h^{-1} are shown in Figure S1.

To place the rain rate distribution in broader context, we show in Figure 4 a set of three climatological maps: (a) the mean rain rate of the events in the top half of the cumulative contribution curve, (b) the frequency of

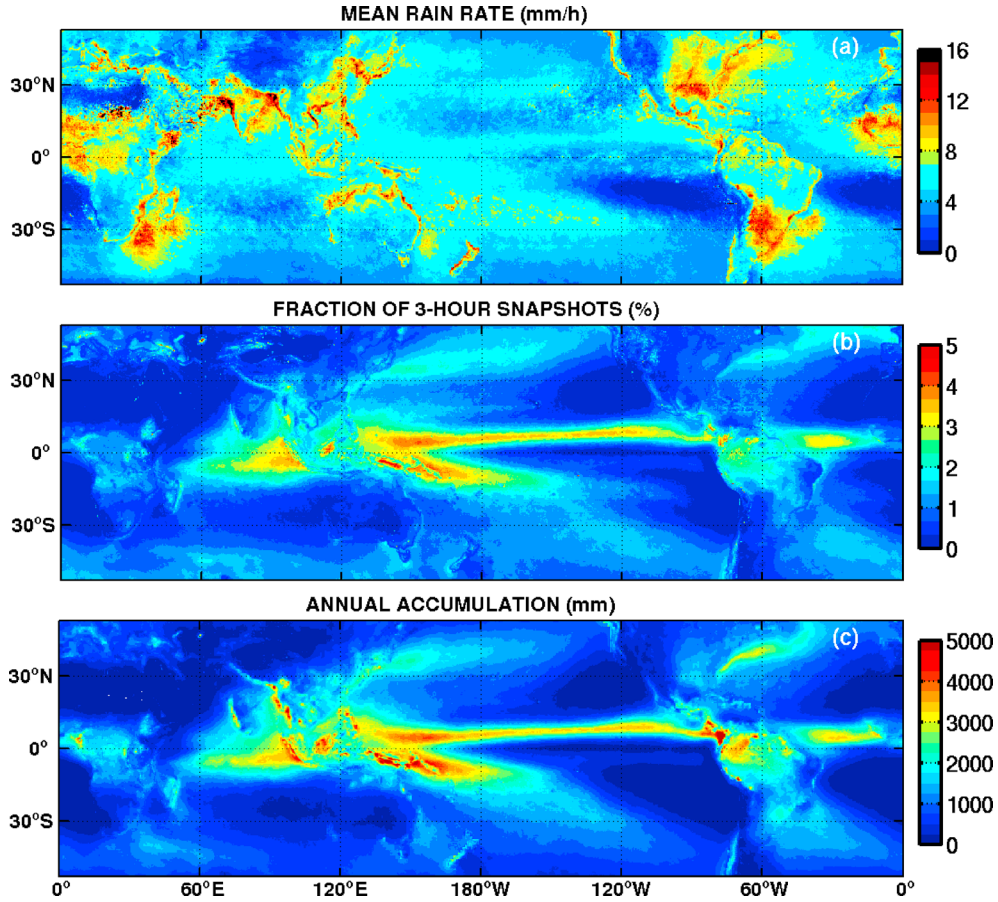

Figure 4. (a) Average rain rate (mm/h) of rain occurrences and (b) time (expressed as a percentage of the 2920 3-hour snapshots) required to account for 50% of the total annual accumulation at each grid point. (c) Total annual accumulation (mm). The product of the metrics shown in the top two panels (× 2920 × 3 h) equals half of the annual accumulation. Based on 15 years (1998–2012) of TRMM 3B42V7 (0.25° × 0.25°, 3-hourly) rainfall data.

occurrence of the rain events in the top half of the cumulative contribution curve expressed as a percentage of the 2920 (3-hourly) snapshots, and (c) the annual mean rainfall. For each grid box, (a) × (b) = (c)/2. From a comparison of these plots it is evident that frequency of rain events is much more important than rain rate in determining the annual mean rainfall. There is no systematic relationship between (conditional) rain rate and rain frequency: both tend to be higher in the oceanic convergence zones than in the belts to the north and south of them, but some of the regions with the highest mean (conditional) rain rates, such as sub-Saharan Africa, experience rain events only rarely.

Many of the coastlines stand out clearly in the rain rate and rain frequency maps. Along many coastlines downwind of the trades, rain rates are enhanced in a narrow strip of grid boxes along the coastline. Along some coastlines such as China and Vietnam, the enhanced rain rates are accompanied by reduction in rain frequencies. Along the east Atlantic coast of South America and the west coast of India, rain frequencies are higher offshore than onshore.

The regions of highest rain frequency are over the oceans. The Pacific and Atlantic equatorial cold tongues in sea surface temperature stand out much more clearly in frequency than in rain rate, and the dry zones exhibit features that are not apparent in rain rate or accumulation. In the South Pacific, the dry zone is split into two WNW-ESE oriented bands that intersect the South American coast near 18°S and 30°S, separated by a narrow zone of more frequent rain occurrences extending out of the south Pacific Convergence Zone (SPCZ), and there are indications of analogous features in the North Pacific and the South Atlantic.

The histogram of climatological R_{50} shown in Figure 5 provides additional support for describing tropical rain rates in terms of regimes based on their spectra as in Figure 2d, as opposed to treating them as a continuum.

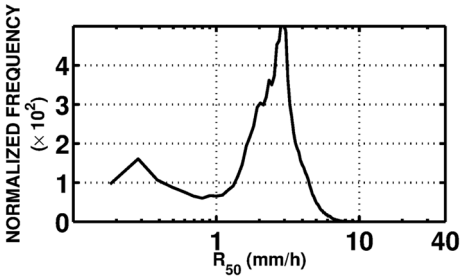

Figure 5. Normalized frequency histogram of the 50% intercept rain rate R_{50} (mm h^{-1}) for the tropics (30°S–30°N), whose spatial pattern is shown in Figure 3a.

The primary peak around 3 mm h^{-1} corresponds to M (the oceanic convergence zones) and the secondary peak ~0.3 mm h^{-1} to L (the subtropical dry zones). Grid boxes categorized as H and V fall within the positive tail of the distribution.

5. Sensitivity to Seasonality and Record Length

In arid regions rain is a rare event, but when it occurs it may involve a high rain rate. Within an interval as short as the 15 year TRMM climatology, not every grid box that is subject to the occurrence of heavy rain will have experienced one or more of these events. Hence, rain rates for grid boxes in arid regions could conceivably be classified as either V or L, depending upon sampling variability. The longer the climatology, the greater the likelihood that any given grid box will have experienced heavy rain and that that box will be categorized as V. A telltale sign of this inherent ambiguity is the patchiness of the patterns of rain rate, with V and L grid boxes interspersed in what would otherwise seem to be a homogeneous climatic region. Consistent with this expectation, the GPM rain rate maps shown in Figures S2 and S3, which are based on a year-long climatology at this point, exhibit considerable patchiness over arid regions. Rain rate climatologies based on TRMM PR data [e.g., *Biasutti and Yuter*, 2013] exhibit a similar patchiness because of the limited sampling of the occurrences of rain in arid and semiarid regions. Rain rate climatologies based on 5 year segments of the TRMM record, shown in Figure S5, are also patchier over arid regions than their counterpart based on the full 15 year climatology shown in Figure 4a but not so much so as to invalidate the utility of conditional rain rate as a parameter for characterizing rainfall climatology.

Many regions of the tropics experience most of their annual rainfall during a rainy season that lasts only a few months. We have examined seasonal climatologies for July–September and December–March (not shown) and found that the rain rate maps for the rainy season mirror the features shown in Figure 3a or 4a based on data for all calendar months. Inclusion of the dry season has little effect on the results. Differences between the rain rate statistics for monsoon and pre/post monsoon seasons, documented by *Biasutti and Yuter* [2013] using TRMM-PR data, would be interesting to explore using 3B42.

6. Summary and Discussion

We have shown in Figure 1 that half the tropical (30°N–30°S) rain falls in ~1% of the area in the TRMM 3B42 (0.25° × 0.25°) data and ~0.5% of the area in the GPM (0.1° × 0.1°) data. It seems likely that the corresponding percentage in the TRMM PR data, with a horizontal resolution of only a few kilometers, would be even smaller. Our estimates are lower than the value of 3% estimated by *Yang and Nesbitt* [2014] on the basis of TRMM PR data because we are accounting for only half the tropical rainfall.

We have shown that over the tropics, the distribution of contribution-weighted rain rate is nearly lognormal, with a peak around 3 mm h^{-1} and that it lends itself to being represented as a "rain rate spectrum," with area under the curve proportional to fractional contribution to total annual rainfall. Most of the diversity of the distributions for individual grid boxes can be characterized in terms of a single parameter, the 50% intercept. Variations in this parameter are a measure of what *Pendergrass and Hartmann* [2014] referred to as a "shifting mode" in the distribution of rain. The logarithmic-mean rain rate, $\overline{R_L}$, exhibits a very similar geographical distribution (Figures 3a and 3b), as do the frequencies of heavy or even extreme rain events based on various exceedance criteria (Figures 3c and S1). These patterns are robust with respect to sampling variability (Figures S4 and S5).

Compared to rain rate statistics from TRMM PR data presented in *Biasutti and Yuter* [2013], our patterns based on the merged data set are much more detailed, particularly over land, by virtue of their nearly 20 times greater sample size. They resolve localized, orographically forced features and provide much more realistic rain rate statistics in regions that experience heavy rain events but only rarely. In describing the rain rate climatology we have found it useful to classify tropical grid boxes in terms of regimes. Twenty two percent of the area of the tropics is classified as light L and 64% as moderate M, which correspond to peaks in the

histogram of climatological-median rain rate shown in Figure 5. L corresponds to a convectively stable region that experiences only stratiform rain events in the climatology, M encompasses widespread but relatively gentle convective rain events, and the remainder of the tropical grid boxes are classified as heavy H (12%) or very heavy V (2%) (Figure 2b).

Features of interest in the heavy and very heavy rain rate regimes (Figures 2b, 3, and 4a) include the following:

1. Offshore regions of relatively high sea surface temperature at subtropical latitudes to the east of South Africa, Australia, and Argentina regions also marked by a high incidence of lightning [*Virts et al.*, 2013] and by local maxima in the frequency of occurrence of wide convective cores with strong thresholds in TRMM PR data [*Houze et al.*, 2015, Figure 5d].
2. Coastal zones. *Ogino et al.* [2016] have noted a tendency for enhanced rainfall close to coastlines in the TRMM data, and our rain rate maps provide further evidence of the narrowness and pervasiveness of these coastal features. Figures S2 and S3, based on the higher resolution GPM data, show that they tend to be centered just offshore rather than on the coastline itself. *Houze et al.* [2015] showed in their Figure 4 that these are zones of strong low level convergence associated with the deceleration of the trade winds as they approach a coastline, where the frictional drag abruptly increases.
3. Valleys upwind of high terrain in which the upslope flow is rendered confluent by the orography, resulting in persistent deep convective clouds with very heavy rain rates. *Liu* [2011] noted similar features in the percentage of the rainfall contributed by events that lasted 12 hours or longer.
4. Along the margins of deserts such as parts of the Sahel and the Horn of Africa, where many of the rain events are in the form of heavy downpours.

Notable rain rate maxima include the zones of very high climatological-mean convective available potential energy (CAPE) over the coastal lowlands adjacent to the Arabian Sea and the Bay of Bengal [e.g., *Riemann-Campe et al.*, 2009] and the more diffuse maximum over northern Argentina, the focus of a recent investigation by *Rasmussen et al.* [2016] based on TRMM PR data. That the highest rain rates tend to be observed over land in the regions listed above is already well established on the basis of studies based on the TRMM PR, e.g., as discussed in *Houze et al.* [2015]. What is new and noteworthy in our results based on the merged TRMM product is (i) how clearly these regions stand out above the more gentle marine convection in climatological spatial patterns of rain rate and (ii) how inhomogeneous rain rates are over land.

7. Concluding Remarks

The spatial patterns of rain rate in our Figures 3 and 4 are broadly consistent with the findings of *Biasutti and Yuter* [2013] and *Yang and Nesbitt* [2014] based on TRMM PR data, but they are substantially more detailed, especially over arid land regions where many more heavy rain events are sampled in the 3B42 climatology. Figures S2 and S3 provide a preview of a higher resolution rain rate climatology based on data from GPM. The record is not yet long enough to provide reliable rain rate statistics for the more arid regions, but with its half hourly sampling rate we can expect that 5 years from now GPM will have sampled as many heavy rain events as TRMM did in its 15 year lifetime.

If rainfall is indeed tending to become more concentrated in a smaller number of heavy events [e.g., *Groisman et al.*, 2005], it should be reflected in an upward trend of rain rate, which is arguably a more robust statistic than those based on exceedance thresholds. The TRMM 3B42 data cannot be used for evaluating trends because the satellite-based observing system evolved substantially during the period of the mission. However, hourly rainfall data from airports and other sites as in the gridded data set for the United States compiled by *Higgins et al.* [1996] may be suitable for this purpose, given the availability of a sufficient number of long, high-quality records from tropical sites. It is worth noting here that while our analysis might be best suited for smaller time/space scales, it could also be applied effectively on daily (or even in situ) observations despite their less than optimal sampling characteristics.

Viewing tropical rainfall from a macroscale perspective and partitioning the variability into contributions related to rain rate and rain frequency raises a number of new questions, such as the following:

1. Why is the convergence of the trade wind flow, as it approaches coastlines, expressed mainly in the form of an enhanced rain rate whereas the ITCZ and SPCZ are expressed mainly as maxima in rain frequency?
2. Why is there an apparent splitting of the oceanic dry zones in rain frequency (Figure 4b) but not in rain accumulation (Figure 4c)?

3. Is the signature of tropical cyclones discernible in the rain rate or the rain frequency climatologies?
4. How do the El Niño–Southern Oscillation, the Madden Julian Oscillation, other tropical waves, and diurnal variations modulate rain rate versus the frequency (or areal coverage) of rain?
5. Are there robust statistical relationships between rain rate and thermodynamic variables such as CAPE, as suggested in *Lepore et al.* [2014] from their analysis of data on very heavy rain events over the United States?

The horizontal resolution of numerical weather prediction models is now comparable to that of the TRMM 3B42 data set. Hence, it should be straightforward to compile rain rate and rain frequency climatologies from forecast model data sets that can be compared directly with the merged data sets based on TRMM and GPM, using the methodologies described here and in *Pendergrass and Hartmann* [2014]. Such comparisons would provide simple yet informative metrics for assessing the fidelity of the parameterization schemes in the models in simulating tropical convection.

Acknowledgments
This work was supported in part by the U.S. National Science Foundation under grant AGS-1122989 and IITM/MAS/DSG/0001 grant MM/SERP/IISc-Bangalore/2014/IND-8/002 under Monsoon Mission funded by the Ministry of Earth Sciences, India. We thank the TRMM science data and information system (TSDIS) and the Goddard Distributed Active Archive Center (DAAC) for providing us the TRMM data.

References

Adler, R. F., G. J. Huffman, D. T. Bolvin, S. Curtis, and E. J. Nelkin (2000), Tropical rainfall distributions determined using TRMM combined with other satellite and rain gauge information, *J. Appl. Meteorol.*, *39*, 2007–2023.
Biasutti, M., S. E. Yuter, C. D. Burleyson, and A. H. Sobel (2012), Very high resolution rainfall patterns measured by TRMM precipitation radar: Seasonal and diurnal cycles, *Clim. Dyn.*, *39*, 239–258.
Biasutti, M., and S. E. Yuter (2013), Observed frequency and intensity of tropical precipitation from instantaneous estimates, *J. Geophys. Res. Atmos.*, *118*, 9534–9551, doi:10.1002/jgrd.50694.
Chokngamwong, R., and L. S. Chiu (2008), Thailand daily rainfall and comparison with TRMM products, *J. Hydrometeorol.*, *9*, 256–266.
Dai, A. (2001), Global precipitation and thunderstorm frequencies. Part I: Seasonal and interannual variations, *J. Clim.*, *14*, 1092–1111.
Dinku, T., P. Ceccato, E. Grover-Kopec, M. Lemma, S. J. Connor, and C. F. Ropelewski (2007), Validation of satellite rainfall products over East Africa's complex topography, *Int. J. Climatol.*, *28*, 1503–1526.
Groisman, P. Y., R. W. Knight, D. Easterling, T. Karl, G. C. Hegerl, and V. N. Razuvaev (2005), Trends in intense precipitation in the climate record, *J. Clim.*, *18*, 1326–1350.
Higgins, R. W., J. E. Janowiak, and Y.-P. Yao (1996), A gridded hourly precipitation database for the United States (1963–1993), in *NCEP/Climate Prediction Center Atlas*, vol. 1, p. 47, National Weather Service, NOAA, U.S. Department of Commerce, Camp Springs, Md.
Hou, A., R. Kakar, S. Neeck, A. A. Azabarzin, C. D. Kummerow, M. Kojima, R. Oki, K. Nakamura, and T. Iguchi (2014), Global Precipitation Mission, *Bull. Amer. Meteorol. Soc.*, *95*, 701–722.
Houze, Jr., R. A., K. L. Rasmussen, M. D. Zuluaga, and S. R. Brodzik (2015), The variable nature of convection in the tropics and subtropics: A legacy of 16 years of the Tropical Rainfall Measuring Mission satellite, *Rev. Geophys.*, *53*, 994–1021, doi:10.1002/2015RG000488.
Huffman, G. J., R. F. Adler, D. T. Bolvin, G. Gu, E. J. Nelkin, K. P. Bowman, Y. Hong, E. F. Stocker, and D. B. Wolff (2007), The TRMM multi-satellite precipitation analysis: Quasi-global, multi-year, combined-sensor precipitation estimates at fine scale, *J. Hydrometeorol.*, *8*, 38–55.
Huffman, G. J., and D. T. Bolvin (2013), TRMM and other data precipitation data set documentation, Lab. for Atmos., NASA Goddard Space Flight Cent. and Sci. Syst. and Appl. [Available at http://precip.gsfc.nasa.gov/pub/trmmdocs/3B42_3B43_doc.pdf.]
Huffman, G. J., D. T. Bolvin, and E. J. Nelkin (2015), Integrated Multi-satellitE Retrievals for GPM (IMERG) technical documentation, NASA Goddard Space Flight Center. [Available at http://pmm.nasa.gov/sites/default/files/document_files/IMERG_doc.pdf.]
Lepore, C., D. Veneziano, and A. Molini (2014), Temperature and CAPE dependence of rainfall extremes in the eastern United States, *Geophys. Res. Lett.*, *42*, 74–83, doi:10.1002/2014GL062247.
Liu, C. (2011), Rainfall contributions from precipitation systems with different sizes, convective intensities, and durations over the tropics and subtropics, *J. Hydrometeorol.*, *12*, 394–412.
Liu, C., and E. Zipser (2015), The global distribution of largest, deepest, and most intense precipitation systems, *Geophys. Res. Lett.*, *42*, 3591–3595, doi:10.1002/2015GL063776.
Ogino, S.-Y., M. D. Yamanaka, S. Mori, and J. Matsumoto (2016), How much is the precipitation amount over the tropical coastal region, *J. Clim.*, *29*, 8357–8371.
Pendergrass, A., and D. L. Hartmann (2014), Two modes of change of the distribution of rain, *J. Clim.*, *27*, 8357–8371.
Rahman, S. H., D. Sengupta, and M. Ravichandran (2009), Variability of Indian summer monsoon rainfall in daily data from gauge and satellite, *J. Geophys. Res.*, *114*, D17113, doi:10.1029/2008JD011694.
Rasmussen, K. L., M. M. Chaplin, M. D. Zuluaga, and R. A. Houze, Jr. (2016), Contribution of extreme convective storms to rainfall in South America, *J. Hydrometeorol.*, *17*, 353–367.
Riemann-Campe, K., K. Fraedrich, and F. Lunkeit (2009), Global climatology of Convective Available Potential Energy (CAPE) and Convective Inhibition (CIN) in ERA-40 reanalysis, *Atmos. Res.*, *93*, 534–545.
Roca, R., P. Chambon, I. Jobard, P.-E. Kirstetter, M. Gosset, and J. C. Berge (2011), Comparing satellite and surface rainfall products over West Africa at meteorologically relevant scales during the AMMA campaign using error estimates, *J. Appl. Meteorol.*, *49*, 715–731.
Sapiano, M. R. P., and P. A. Arkin (2009), An intercomparison and validation of high-resolution satellite precipitation estimates with 3-hourly gauge data, *J. Hydrometeorol.*, *10*, 149–166.
Simpson, J., C. Kummerow, W. K. Tao, and R. F. Adler (1996), On the Tropical Rainfall Measuring Mission (TRMM), *Meteorol. Atmos. Phys.*, *60*(1), 19–36.
Trenberth, K., A. Dai, R. Rasmussen, and D. Parsons (2003), The changing character of precipitation, *Bull. Amer. Meteorol. Soc.*, *84*(9), 1205–1217.
Virts, K. S., J. M. Wallace, M. L. Hutchins, and R. H. Holzworth (2013), The changing character of precipitation, *Bull. Amer. Meteorol. Soc.*, *94*, 1381–1391.
Watterson, I., and M. Dix (2003), Simulated changes due to global warming in daily precipitation means and extremes and their interpretation using the gamma distribution, *J. Geophys. Res.*, *108*, 4379–4398, doi:10.1029/2002JD002928.
Yang, S., and S. W. Nesbitt (2014), Statistical properties of precipitation as observed by the TRMM Precipitation Radar, *Geophys. Res. Lett.*, *41*, 5636–5643, doi:10.1002/2014GL060683.